

Vertical organic spin valves in perpendicular magnetic fields

M. Grünewald,^{1,2} R. Göckeritz,² N. Homonnay,² F.
Würthner,^{3,4} L.W. Molenkamp,^{1,3} and G. Schmidt^{1,2,*}

¹*Physikalisches Institut (EP3), Universität Würzburg,
Am Hubland, D-97074 Würzburg, Germany*

²*Institute of Physics, Martin-Luther-Universität Halle-Wittenberg,
Von-Danckelmann-Platz 3, D-06120 Halle, Germany*

³*Röntgen Center for Complex Material Systems,
Universität Würzburg, Am Hubland, D-97074 Würzburg, Germany*

⁴*Institut für Organische Chemie, Universität Würzburg,
Am Hubland, D-97074 Würzburg, Germany*

Abstract

We report the results of magnetoresistance measurements in vertical organic spin valves with the magnetic field oriented perpendicular to the layer stack. The magnetoresistance measurements were performed after carefully preparing either parallel or antiparallel in-plane magnetization states of the magnetic electrodes in order to observe traces of Hanle precession. Due to the low mobility in organic semiconductors the transit time of spin polarized carriers should allow for precession of the spins in perpendicular fields which in statistical average would quench the magnetoresistance. However, in none of the experiments we do observe any change in resistance while sweeping the perpendicular field, up to the point where the electrode's magnetization starts to reorient. This absence of Hanle type effects indicates that the magnetoresistance is not based on the injection of spin polarized electrons into the organic semiconductor but rather on tunneling through pinholes superimposed with tunneling anisotropic magnetoresistance.

PACS numbers: 81.05.Fb, 72.25.-b, 75.76.+j

I. INTRODUCTION

A number of experiments using vertical organic spin valves (OSVs) have been demonstrated over the past years, for example Refs. [1–8]. In many cases it is still unclear whether a tunneling based magnetoresistance effect (TMR/TAMR)^{6,8,9} or actual spin injection and consequently giant magnetoresistance (GMR)^{2,7} is the origin of the observed effects. Although the investigation of I/V-characteristics or the temperature dependence of the device resistance can give indications about the underlying transport mechanisms, final proof is still missing. Further complications arise from the facts that charge injection into organic semiconductors is often based on tunneling¹⁰ and that intermixing of spin dependent transport and tunneling anisotropic magnetoresistance⁹ can prevent a clear distinction between TMR and GMR.

In the advent of electrical spin injection into inorganic semiconductors a similar problem existed. Especially in high mobility semiconductors stray magnetic fields originating from magnetic contacts can modulate intrinsic magnetoresistance effects and thus mimic the signature of spin injection. For electrically detected spin injection in inorganic semiconductors the final litmus test was the investigation of Hanle precession in perpendicular magnetic fields^{11,12}. It can easily be shown that the principle of Hanle precession^{13,14} is also applicable for organic spin valves, though with a slightly different result.

The Hanle effect itself is based on the precession of spins with the Larmor frequency ω_L induced by a magnetic field B which is oriented perpendicular to the spin:

$$\omega_L = \frac{egB}{2m_e} \quad (1)$$

m_e is the electron rest mass, g the electron's g -factor. Thus the spin \vec{s} (phase φ_0 at time $t = 0$) becomes time-dependent and can be described by:

$$\vec{s} = \frac{1}{2}\hbar \begin{pmatrix} \cos(\varphi_0 + \omega_L \cdot t) \\ \sin(\varphi_0 + \omega_L \cdot t) \end{pmatrix} \quad (2)$$

Usually spin polarized transport in organic or inorganic semiconductors is demonstrated in devices consisting of a non-magnetic transport layer placed between at least two ferromagnetic electrodes in a lateral or vertical arrangement, so called spin valve devices. The resistance R of a spin valve device depends on the relative magnetization of the

electrodes (antiparallel R_{AP} /parallel R_P). Provided that the electrodes exhibit different coercive fields, R therefore can be adjusted by a magnetic field B_{ip} which is applied in the sample plane.

If in a spin valve device spins actually are injected into the non-magnetic spacer layer the Hanle effect can cause a change of the measured signal (device resistance/current). The spins then precess in a magnetic field B_z applied perpendicular to the sample plane while the in-plane field B_{ip} is kept constant at zero. This precession changes the relative orientation of the spins with respect to the magnetization of the electrodes. This change of the spins' direction has the same consequences as a change of the electrodes magnetization and therefore can be detected in the measured signal.

The results that can be obtained in a specific experiment investigating the presence of the Hanle effect may be varying depending on the transport characteristics of the material under investigation. However the Hanle effect always appears as spin-dephasing if rather large magnetic fields B_z are applied. When B_z , which causes the spin precession, is increased ω_L also gets larger, i.e. the precession gets faster. If ω_L is sufficiently high the single spins perform several full precessions during their transit through the layer under investigation. As the time t_{trans} which is needed for the transit through this layer cannot be the same for every single spin in the material the spin-polarization of the total current averages out due to the precession. This loss of spin-polarization usually is called spin-dephasing^{11,15}. In materials in which the spin transport occurs rather incoherently, i.e. the variation in t_{trans} is large, spin-dephasing can already be observed at small B_z resulting in a simple quenching of the magnetoresistance. In contrast, if coherent spin transport is present large B_z must be applied in order to observe the decrease in magnetoresistance while the coherent precession is observed as so called Hanle oscillations¹² of the resistance.

Fig. 1 shows resistance traces that can be expected for measurements in perpendicular magnetic fields in a spin valve device in which the Hanle effect is present and incoherent transport is dominating. To initialize this kind of measurement, it is necessary to prepare the parallel (antiparallel) state resulting in a device resistance of R_P (R_{AP}) at $B_{ip} = 0$ before the sweep of B_z is started. For a spin valve for which $R_P > R_{AP}$ as is

typical for organic spin valves increasing B_z results in a decrease of R_P and in an increase of R_{AP} . Both curves end up at the same intermediate resistance R_{int} at sufficiently large B_z .

It should be noted here that the observation of the Hanle effect is the most robust proof for electrical spin injection and detection. Other methods to demonstrate the injection of spin polarized carriers like faraday rotation in inorganic semiconductors¹⁶ or muon spin rotation¹⁷ or two photon photoemission¹⁸ in organic semiconductors (OSCs) can be used as a proof for spin injection, however, they cannot check whether an electrically detected spin valve signal originates from spin polarized carrier transport or from side effects. Only the Hanle effect provides the necessary proof that the signal truly originates from the electrical detection of spin polarized carriers. Thus the investigation of the Hanle effect by magnetoresistance measurements (MR) in perpendicular magnetic fields (also named perpendicular geometry hereafter) is an indispensable tool to interpret and understand the results of any spin valve experiment.

So far, most of the experiments in which Hanle effect and electrical spin injection is observed are reported for lateral spin valve devices with inorganic spacers (Si, GaAs, Graphene). Our experiments comprise magnetoresistance measurements in perpendicular magnetic fields on a number of OSV devices with a layer of an OSC as the spin transporting material sandwiched between two ferromagnetic electrodes where the bottom electrode consists of $La_{0.7}Sr_{0.3}MnO_3$ (LSMO) and the top electrode is a ferromagnetic metal. The vertical arrangement of the devices functional layers as well as the choice of LSMO and Co or Co alloys as electrode materials is common to nearly all OSVs reported so far.

In the discussion about the Hanle effect in vertical spin valves two arguments are often brought forward in order to explain the possible absence of spin precession: Firstly B_z might be shielded by the ferromagnetic electrodes' layers in the vertical geometry thus impeding the spin precession by reducing B_z to zero. Secondly the thickness of the OSC layer is usually small compared to the length of a spin-conducting channel in lateral spin valve devices. As a consequence the spin transfer from one electrode to the other (e.g. represented by the transit time t_{trans}) might occur on a timescale much shorter than the precession time of the spins if a perpendicular field in the $< 1\text{ T}$ regime is applied.

We can, however, rule out these unwanted effects in our devices for two reasons. First the high in-plane shape anisotropy of ferromagnetic thin films resulting from their large volume magnetization ($\approx 600 \text{ emu/cm}^3$ for LSMO¹⁹, $\approx 1400 \text{ emu/cm}^3$ for Co²⁰ and $\approx 1500 \text{ emu/cm}^3$ for CoFe²¹) has to be taken into account. Due to this shape anisotropy the magnetization remains completely in-plane, even for small perpendicular fields, preventing any shielding of B_z .

For the transit time the following estimation shows that indeed only rather small B_z are needed for a sufficiently fast precession of the spins. Assuming $g = 2$ for any OSC the precession time t_{prec} can be calculated from Equ. 1

$$t_{prec} = \frac{2\pi m_e}{eB_z} \quad (3)$$

This yields $t_{prec} \approx 36 \text{ ns}$ for $B_z = 1 \text{ mT}$. t_{prec} has to be compared to the transit time which is needed for a spin to travel through the OSC layer with a thickness d_{OSC} . We make a rough estimation for t_{trans} as well:

$$t_{trans} = \frac{d_{OSC}}{v} = \frac{d_{OSC}}{\mu E} = \frac{d_{OSC}^2}{\mu U_{bias}} \quad (4)$$

v is the velocity of the spins, E the electric field. Typical values for an OSV experiment are: mobility $\mu = 1 \cdot 10^{-3} \text{ cm}^2/Vs$, $d_{OSC} = 100 \text{ nm}$ and applied bias voltage $U_{bias} = 100 \text{ mV}$. With these values we obtain $t_{trans} = 1 \mu s \approx 30 \cdot t_{prec}$ from Equ. 4. Thus even for thin OSC layers the precession at small B_z is sufficiently fast compared to the transit time to cause a spin-dephasing effect. At the same time the perpendicular field itself is far too weak to be shielded by the ferromagnetic electrodes. It should be noted that the mobility used for the calculation is an upper estimate and the mobilities that we expect to obtain in the experiment are considerably lower.

Furthermore we conclude from the comparison of t_{prec} and t_{trans} that the transport through the OSC layer is so slow that we do not expect to see any Hanle oscillations but only the Hanle effect caused by the spin-dephasing (see Fig. 1). This conclusion is additionally sustained by the fact that the charge transport in amorphous or polycrystalline

OSC layers is occurring by rather incoherent mechanisms like variable range hopping²² or multiple trapping and release²³.

Although no Hanle effect as such has been observed in organic semiconductors, the demonstration of spin precession of conduction electrons in OSC by paramagnetic resonance²⁴ clearly shows that the underlying physics is the same for organic and inorganic semiconductors.

II. EXPERIMENTAL DETAILS

We have fabricated two sets of vertical spin valve structures with different OSC materials as spacer layer which are also different concerning the electrodes and the fabrication process.

The first material under investigation is the *n*-type OSC *N,N'*-bis(*n*-heptafluorobutyl)-3,4:9,10-perylene tetracarboxylic diimide [PTCDI-C4F7, Fig. 2(b)] which is used due to its excellent properties with respect to charge carrier mobility and stability in ambient conditions²⁵. PTCDI-C4F7 is a material well suited for spin valve applications as already has been shown in our previous work⁹. The devices based on this material have a bottom contact made of 10 – 20 *nm* thick LSMO layers, grown by pulsed plasma deposition²⁶ on Strontium Titanate (STO) or Neodymium Gallate (NGO) substrates, and a CoFe top contact. A series of devices with different OSC layer thicknesses d_{OSC} ranging from 100 *nm* to 600 *nm* was fabricated.

For device fabrication with PTCDI-C4F7 as OSC spacer, first Ti/Au metal stripes are deposited on the LSMO, using optical lithography, evaporation, and lift-off. These stripes serve as alignment marks and later as bondpads. A rectangular bottom contact is then patterned into the LSMO layer by optical lithography and dry etching, leaving the metal contact at one side of the rectangle. Subsequently, the sample is inserted into the UHV-deposition chamber where a bake-out procedure is performed at 450 °C for 1 hour at an oxygen pressure of 10^{-5} mbar, in order to compensate under-oxygenation which may occur during the processing. Subsequently, the PTCDI-C4F7 layer and the metal top electrode are deposited under different angles of incidence through a shadow mask with a

rectangular opening. After removing the sample from the UHV chamber, Ti/Au stripes are deposited through a second shadow mask with striped windows. These metal stripes are later used as bond pads for the top contacts and also serve as an etch mask for the removal of the top electrode material between the stripes by dry etching. This approach provides clean, oxygen-free, and reproducible interfaces which are known to be crucial for working OSV devices.

Furthermore we also fabricated devices with the well known and extensively investigated material Tris(8-hydroxyquinoline)-aluminium(III) [AlQ₃, Fig. 2(a)], a low mobility amorphous *n*-type OSC. The fabrication process for these devices is different from the one for the PTCDI-C4F7 devices and will be explained in detail elsewhere. The main differences compared to the PTCDI-C4F7 devices are the fabrication method of the LSMO electrode (thickness 20 nm, grown by pulsed laser deposition) and the patterning of the devices' active area by means of lithography instead of shadow masks and dry etching. The thickness of the OSC layer is ranging from 40 nm to 100 nm for the AlQ₃ devices.

The samples are characterized at various temperatures between 4.2 K and room temperature. Preliminary investigations of the observed MR effects were done in either in a ⁴He flow cryostat or a ⁴He bath cryostat, both equipped with an external room temperature electromagnet ($B_{max} = 600\text{ mT}$ respectively $B_{max} = 800\text{ mT}$) at various temperatures. The experiments in the perpendicular geometry were conducted at 4.2 K in a ⁴He bath cryostat with a 3D vector magnet in which magnetic fields up to 400 mT can be applied in any direction in space.

III. RESULTS

A. SPIN VALVE EFFECTS

Fig. 2 shows typical magnetoresistance traces for both types of devices. The magnetoresistance trace of an AlQ₃ based device (present device: $d_{OSC} = 50\text{ nm}$) is shown in Fig. 2(a). The actual spin valve signal is very pronounced and almost no background effect is observed,

only a small decrease of R with increasing B_{ip} can be discerned. The spin valve effect itself is negative (low resistance state appears for parallel magnetization of the electrodes R_{AP}). The change of the magnetization can be identified as sharp switching events in the MR trace. When B_{ip} is swept from high positive to high negative fields the first switching event leading to the low resistance state R_{AP} appears at small negative fields ($B_{ip} \approx -10 \text{ mT}$). This switching can be ascribed to the magnetization reversal of the LSMO electrode. The Co electrode's magnetization is reversed at higher fields ($B_{ip} \approx -100 - -200 \text{ mT}$) via multiple steps finally resulting in the high resistance parallel magnetization state R_P again. The MR effect has a magnitude of $\text{MR} = (R_{AP} - R_P)/R_{AP} \approx -2.0 \%$ at 4.2 K and $U_{bias} = -100 \text{ mV}$ and is symmetric with respect to $B_{ip} = 0 \text{ mT}$, i.e. for the opposite sweep direction the same behavior is observed in the positive field range, .

The magnetoresistance trace of a PTCDI-C4F7 based device (present device: $d_{OSC} = 150 \text{ nm}$) has a different shape [Fig. 2(b)]. The observed effect with a total MR ratio of $\approx -20 \%$ at 4.2 K and $U_{bias} = -10 \text{ mV}$ again is symmetric with respect to $B_{ip} = 0 \text{ mT}$ but has two distinct components. On one hand the MR trace comprises a non-linear background effect, increasing resistance with increasing B_{ip} , which is well known for various OSV devices based on other OSCs reported in the literature^{4,27-29} and can be explained by the magnetic electrodes being saturated at higher magnetic fields. The Organic Magnetoresistance Effect³⁰ (OMAR) can be excluded very likely as origin for the background signal in our devices as has been shown in previous studies⁹. On the other hand we see the actual negative spin valve effect which is less pronounced compared to the AlQ_3 OSV due to the superimposed background signal. Comparable to the AlQ_3 device the first switching event from high (R_P) to low resistance (R_{AP}) occurs at small B_{ip} . When B_{ip} is further increased the magnetization reversal of the second electrode (CoFe) occurs at $B_{ip} \approx -100 \text{ mT}$ which is lower than the magnetic field required to reverse the magnetization of the Co electrode in the AlQ_3 devices.

The spin valve signals presented in Fig. 2 have been studied extensively with respect to various parameters (temperature, U_{bias} , d_{OSC}), which will be presented elsewhere. Nevertheless, these experiments did not yield reliable proof for the underlying transport mechanisms of the observed spin valve effects. As already mentioned above more information can be

gained by measurements in perpendicular magnetic fields.

B. EXPERIMENTS IN THE PERPENDICULAR GEOMETRY: AlQ_3 OSVS

In order to detect the presence of Hanle precession it is necessary to apply the perpendicular magnetic field to the in-plane antiparallel magnetized and the in-plane parallel magnetized states of the spin valve, respectively. The fact that OSV often exhibit a negative spin valve effect shows that sign and magnitude of the spin accumulation in the organic semiconductor cannot be related to the magnetization states in a straightforward manner.

As a consequence it is not possible to predict whether the influence of spin precession on the two individual resistance states is equally strong. It is however obvious that the difference in resistance between the two states should diminish when Hanle precession is present. Thus it is important to investigate both remanent states in detail. In a recent publication³¹, data has already been presented for magnetic field sweeps perpendicular to the sample plane, however, starting the sweep from perpendicular saturation. In our case the use of a 3D vector magnet allows us to prepare both remanent states individually by running a field sweep from parallel saturation to the desired state and then reducing the in-plane field to zero. Subsequently the perpendicular field is applied and swept over the desired range. After the perpendicular field sweep is finished the in plane MR loop is completed in order to verify that the magnetization state of the electrodes is unchanged (the corresponding field sweeps for the preparation of the spin valves' antiparallel and parallel state are shown in Fig. 3).

Fig. 4 summarizes a complete sequence of measurements in the perpendicular geometry for the antiparallel configuration in a AlQ_3 based device. All measurements are performed at $U_{bias} = -100 \text{ mV}$ and $T = 4.2 \text{ K}$. The antiparallel state is prepared by sweeping B_{ip} on a minor-loop [Fig. 4(a) and (b)]: Starting at high positive fields B_{ip} is swept beyond 0 mT (orange/light grey curve) until the magnetization of the LSMO electrode is reversed yielding the low resistance state. Subsequently B_{ip} is set to 0 mT (blue/dark grey curve). As can be seen in Fig. 4(b) the device remains in the low resistance state when B_{ip} is turned off.

Hence a stable remanent antiparallel configuration of the electrodes' magnetization with $R_P \approx 1.575\text{ k}\Omega$ and $R_{AP} \approx 1.55\text{ k}\Omega$ corresponding to minor-loop MR ratio of $\approx -1.7\%$ is prepared.

The measurements with the magnetic field applied perpendicular to the sample plane involve sweeps of B_z from 0 mT to higher fields (up to $\pm 20\text{ mT}$) and back while the in-plane field remains at $B_{ip} = 0\text{ mT}$. Fig. 4(c)-(f) show the results of these experiments. The data uses the same scale as the full magnetoresistance sweep. In each measurement the maximum absolute value of B_z and by this ω_L is increased while the spins' precession time t_{prec} is decreased. t_{prec} is ranging from $t_{prec} \approx 7.1\text{ ns}$ to $t_{prec} \approx 1.8\text{ ns}$ (minimum values calculated from Equ. 3 for the respective maximum value of B_z). In all measurements we obtain, independently of the sweep direction of B_z and its maximum value, a constant device resistance with only statistical variations of $\approx \pm 0.25\%$ around $R(0\text{ mT})$.

After returning B_z to zero the minor-loop we have used to prepare the in-plane antiparallel state is completed. This measurement is done in order to ensure that the electrodes' magnetization has not been modified by the application of B_z and therefore the antiparallel state of the OSV device was not disturbed. The line with the open circles in Fig. 4(g) which shows the data for this measurement clearly reproduces the MR scan for this device recorded without any interruption [Fig. 2(a)]. Furthermore this result also allows us to conclude that the small variations in R observed in the single measurements in Fig. 4(c)-(g) are not caused by any influence of the applied B_z on the electrodes magnetization.

The initialization sequence for the parallel configuration is similar to the minor-loop scan in which the antiparallel state is prepared. For the preparation of the parallel state B_{ip} is swept from saturation in the positive field range to $B_{ip} = 0\text{ mT}$ ending at $R_P \approx 1.575\text{ k}\Omega$ (Fig. 5(a) closed circles).

Fig. 5(b) shows data of one measurement in the perpendicular geometry with a maximum B_z of $\pm 5\text{ mT}$ which is done for the parallel state. This corresponds to a minimum precession time of $t_{prec} \approx 7.1\text{ ns}$. Obviously we do not observe any sizeable change of the OSV's resistance for this configuration as well. After the sweep of B_z the

MR loop is completed similarly as for the antiparallel state. The data of this measurement is shown in 5(a) (open circles) again reproducing the previously recorded full MR trace.

With a minimum precession time of $t_{prec} \approx 1.8 \text{ ns}$ we are clearly in a limit where the magnetoresistance should be quenched completely by the Hanle effect. The fact that the observed variations in perpendicular fields are statistical and much smaller than the total magnetoresistance clearly indicates that no spin polarized charge transport is responsible for the observed magnetoresistance.

C. EXPERIMENTS IN THE PERPENDICULAR GEOMETRY: PTCDI-C4F7 OSVS

For the PTCDI-C4F7 based device similar measurements in perpendicular geometry are performed. Fig. 6a shows the preparation of the antiparallel remanent state by reversing the magnetization of the LSMO layer in a minor loop. As can be seen in the enlarged presentation in Fig. 6(b) the minor-loop MR ratio in this device is $\approx -4.7\%$ when the in-plane field is set back to $B_{ip} = 0 \text{ mT}$. The corresponding resistance values are $R_P \approx 62.5 \text{ k}\Omega$ for the parallel remanent state and $R_{AP} \approx 59.7 \text{ k}\Omega$ for the antiparallel remanent state.

The measurements in the perpendicular geometry are shown in Fig. 6(c)-(g). The maximum absolute values of B_z correspond to precession times $t_{prec} \approx 11.9 - 1.8 \text{ ns}$. The data in Fig. 6(c)-(g) shows that for any value of B_z the device resistance varies by less than $\approx \pm 1\%$. The sweep completing the initial minor-loop, is shown in Fig. 6(h) (line with open circles).

Fig. 7 summarizes the respective experiments in the parallel configuration of the PTCDI-C4F7 device. After sweeping B_{ip} from large positive values to $B_{ip} = 0 \text{ mT}$ (Fig. 7(a), line with closed circles) measurements with the magnetic field applied perpendicular to the sample plane are performed. Obviously the devices resistance has slightly drifted in the time between the measurements for the antiparallel and the parallel state, however this change did not substantially influence the devices spin valve performance as was ensured

by a full MR sweep (Fig. 7(a) blue/dark grey line in the background of the panel). The maximum B_z for the data in Fig. 7(b) is $\pm 5 mT$ corresponding to a precession time of $t_{prec} \approx 7.1 ns$. This data shows that we do not observe any sizeable change of the device's resistance for the parallel configuration as well. Again the measurement is completed by the final sweep of B_{ip} to negative values. (Fig. 7(a), line with open circles). The data of this measurement continues the initial B_{ip} -sweep and reproduces the typical MR trace of the device (Fig. 2(b), blue/dark grey line in Fig. 7(a) respectively).

Although for the PTCDI-C4F7 based device the magnetoresistance trace is less pronounced than for the AlQ_3 based one, the variation of the resistance in the parallel and the antiparallel state, respectively, clearly shows that no Hanle precession can be observed, and thus also in this device spin polarized charge transport is not the cause of the magnetoresistance.

IV. CONCLUSION

We have shown the results of magnetoresistance measurements with the magnetic field applied perpendicular to the sample plane after preparing in-plane parallel or antiparallel magnetization states. The devices under investigation differ in OSC material but also in the shape of the observed spin valve signal. In none of our measurements do we observe any Hanle effect in the perpendicular geometry. Although the observations tell nothing about the possible injection of spin polarized carriers into the organic material we must, as a consequence, exclude any spin-polarized transport through the OSC layer as origin of the observed spin valve effects. Because of the small bias voltages that were used in our experiments we can also exclude fringe-field-induced magnetoresistance that can mimic spin valve signals, however, only at elevated U_{bias} ³². It is thus likely that TMR by tunneling through pinholes superimposed by TAMR occurring at charge injection into the OSC is the cause of the spin valve behavior of our devices.

V. ACKNOWLEDGEMENTS

We thank the EU for funding the research in the projects OFSPIN (NMP-CT-2006-033370) and HINTS (NMP3-SL-2011-263104). We acknowledge Patrizio Grazioso and Alek Dediu from CNR Bologna for provision of the LSMO layer for the PTCDI-C4F7 based OSV device.

* Correspondence to G. Schmidt: georg.schmidt@physik.uni-halle.de

- ¹ V. Dediu, M. Murgia, F. C. Maticotta, C. Taliani, and S. Barbanera, *Solid State Commun.* **122**, 181 (2002).
- ² Z. H. Xiong, D. Wu, Z. V. Vardeny, and J. Shi, *Nature* **427**, 821 (2004).
- ³ S. Majumdar, H. S. Majumdar, R. Laiho, and R. Österbacka, *J. Alloys Compd.* **423**, 169 (2006).
- ⁴ W. Xu, G. J. Szulcowski, P. LeClair, I. Navarrete, R. Schad, G. Miao, H. Guo, and A. Gupta, *Appl. Phys. Lett.* **90**, 072506 (2007).
- ⁵ F. J. Wang, Z. H. Xiong, D. Wu, J. Shi, and Z. V. Vardeny, *Synth. Met.* **155**, 172 (2005).
- ⁶ T. S. Santos, J. S. Lee, P. Migdal, I. C. Lekshmi, B. Satpati, and J. S. Moodera, *Phys. Rev. Lett.* **98**, 016601 (2007).
- ⁷ T. D. Nguyen, G. Hukic-Markosian, F. Wang, L. Wojcik, X.-G. Li, E. Ehrenfreund, and Z. V. Vardeny, *Nat. Mater.* **9**, 345 (2010).
- ⁸ J. J. H. M. Schoonus, P. G. E. Lumens, W. Wagemans, J. T. Kohlhepp, P. A. Bobbert, H. J. M. Swagten, and B. Koopmans, *Phys. Rev. Lett.* **103**, 146601 (2009).
- ⁹ M. Grünwald, M. Wahler, F. Schumann, M. Michelfeit, C. Gould, R. Schmidt, F. Würthner, G. Schmidt, and L. W. Molenkamp, *Phys. Rev. B* **84**, 125208 (2011).
- ¹⁰ M. A. Baldo and S. R. Forrest, *Phys. Rev. B* **64**, 085201 (2001).
- ¹¹ X. Lou, C. Adelmann, S. A. Crooker, E. S. Garlid, J. Zhang, K. S. M. Reddy, S. D. Flexner, C. J. Palmstrom, and P. A. Crowell, *Nat. Phys.* **3**, 197 (2007).
- ¹² B. Huang, D. J. Monsma, and I. Appelbaum, *Phys. Rev. Lett.* **99**, 177209 (2007).
- ¹³ M. Johnson and R. H. Silsbee, *Phys. Rev. Lett.* **55**, 1790 (1985).
- ¹⁴ M. Johnson and R. H. Silsbee, *Phys. Rev. B* **37**, 5326 (1988).
- ¹⁵ N. Tombros, C. Jozsa, M. Popinciuc, H. T. Jonkman, and B. J. van Wees, *Nature* **448**, 571

- (2007).
- ¹⁶ J. M. Kikkawa and D. D. Awschalom, *Nature* **397**, 139 (1999).
 - ¹⁷ A. J. Drew, J. Hoppler, L. Schulz, F. L. Pratt, P. Desai, P. Shakya, T. Kreouzis, W. P. Gillin, A. Suter, N. A. Morley, et al., *Nat. Mater.* **8**, 109 (2009).
 - ¹⁸ M. Cinchetti, K. Heimer, J.-P. Wuestenberg, O. Andreyev, M. Bauer, S. Lach, C. Ziegler, Y. Gao, and M. Aeschlimann, *Nat. Mater.* **8**, 115 (2009).
 - ¹⁹ M. Ziese, I. Vrejoiu, and D. Hesse, *Appl. Phys. Lett.* **97**, 052504 (2010).
 - ²⁰ M. Nishikawa, E. Kita, T. Erata, and A. Tasaki, *J. Magn. Magn. Mater.* **126**, 303 (1993).
 - ²¹ T. Burkert, L. Nordström, O. Eriksson, and O. Heinonen, *Phys. Rev. Lett.* **93**, 027203 (2004).
 - ²² S. M. Sze, *Physics of Semiconductor Devices, Third Edition* (Wiley & Sons, 2006).
 - ²³ G. Horowitz, *Adv. Mater.* **10**, 365 (1998).
 - ²⁴ W. J. Baker, K. Ambal, D. P. Waters, R. Baarda, H. Morishita, K. van Schooten, D. R. McCamey, J. M. Lupton, and C. Boehme, *Nat. Commun.* **3**, 898 (2012).
 - ²⁵ J. H. Oh, S. Liu, Z. Bao, R. Schmidt, and F. Würthner, *Appl. Phys. Lett.* **91**, 212107 (2007).
 - ²⁶ I. Bergenti, V. Dediu, E. Arisi, T. Mertelj, M. Murgia, A. Riminucci, G. Ruani, M. Solzi, and C. Taliani, *Org. Electron.* **5**, 309 (2004).
 - ²⁷ H. Vinzelberg, J. Schumann, D. Elefant, R. B. Gangineni, J. Thomas, and B. Büchner, *J. Appl. Phys.* **103**, 093720 (2008).
 - ²⁸ S. Majumdar, R. Laiho, P. Laukkanen, I. J. Väyrynen, H. S. Majumdar, and R. Österbacka, *Appl. Phys. Lett.* **89**, 122114 (2006).
 - ²⁹ F. J. Wang, C. G. Yang, Z. V. Vardeny, and X. G. Li, *Phys. Rev. B* **75**, 245324 (2007).
 - ³⁰ T. L. Francis, O. Mermer, G. Veeraraghavan, and M. Wohlgenannt, *New J. Phys.* **6**, 185 (2004).
 - ³¹ A. Riminucci, M. Prezioso, C. Pernechele, P. Graziosi, I. Bergenti, R. Cecchini, M. Calbucci, M. Solzi, and V. A. Dediu, *Appl. Phys. Lett.* **102**, 092407 (2013).
 - ³² F. Wang, F. Macià, M. Wohlgenannt, A. D. Kent, and M. E. Flatté, *Phys. Rev. X* **2**, 021013 (2012).

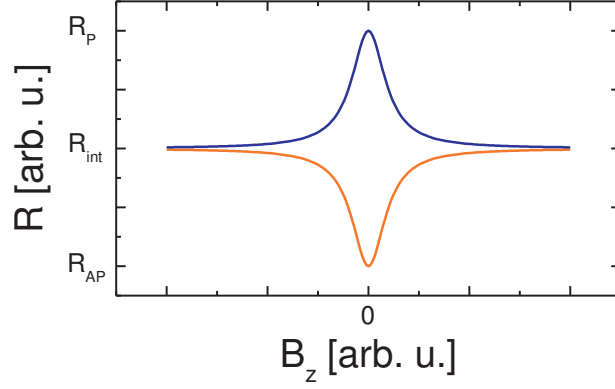


FIG. 1: Theoretical traces of a device's resistance during experiments in a perpendicular magnetic field B_z for the previously prepared parallel (blue, dark grey curve) and antiparallel (orange, light grey curve) spin valve configuration assuming incoherent transport. As with increasing B_z the spin-polarization is decreased due to spin-dephasing the spin valve signal, i.e. the difference of the two curves, is quenched at high B_z . In both measurements, for the antiparallel and parallel state, the same intermediate resistance state R_{int} is reached at high B_z starting at the respective value $R_{AP,P}$ at $B_z = 0$. The data is shown for a spin valve device with a negative effect ($R_{AP} < R_P$) as this behavior is usually observed in organic spin valve devices.

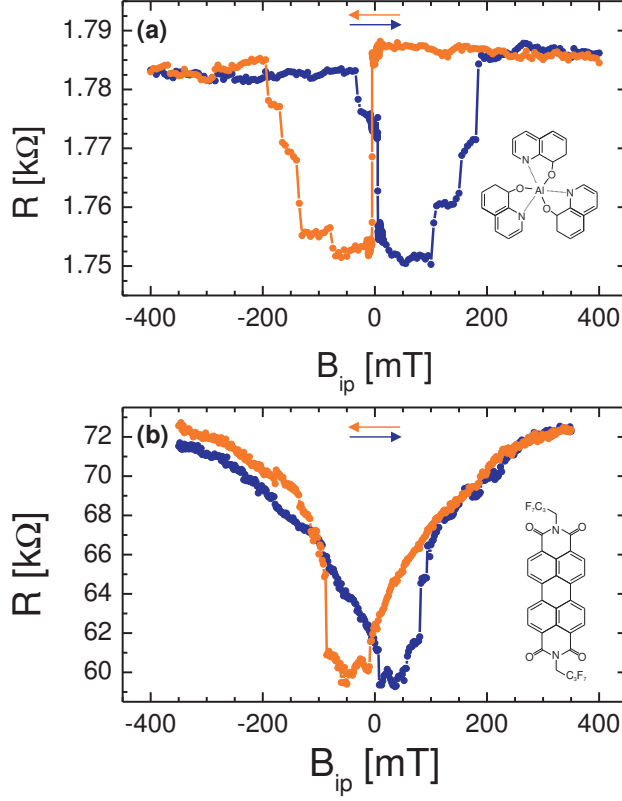


FIG. 2: Typical MR traces for OSV devices of both types. As indicated by the arrows the sweep from positive saturation to negative saturation is represented by the orange/light grey curve, the opposite sweep direction by the blue/dark grey curve. (a) shows the spin valve behavior of a AlQ_3 OSV device ($d_{\text{OSC}} = 50 \text{ nm}$) with a total MR of $\approx -2.0\%$. Only sharp switching events between the parallel and antiparallel configuration and back are observed for this device. The measurement is done at 4.2 K and $U_{\text{bias}} = -100 \text{ mV}$. The MR trace for a PTCDI-C4F7 OSV device ($d_{\text{OSC}} = 150 \text{ nm}$) in (b) with a total MR of $\approx -20\%$ taken at $U_{\text{bias}} = -10 \text{ mV}$ and 4.2 K exhibits spin valve like behavior and a relatively large non-linear background. A constant increase of R with increasing B_{ip} is superimposed to the two distinct switching events between the parallel and antiparallel configuration and back (spin valve signal). The panels also show the molecular structure of the respective OSC material under investigation.

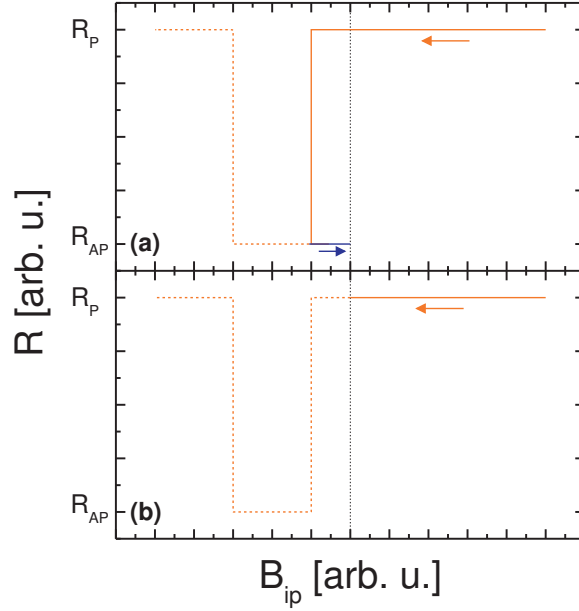


FIG. 3: Schematic presentation of the B_{ip} -sweeps required for the preparation of the antiparallel (a) and parallel (b) magnetization state of a spin valve's electrodes (starting at positive saturation). The solid lines show the sweeps necessary for preparation while the dashed lines represent a complete trace of the negative spin valve signal ($R_{AP} < R_P$). The antiparallel state (a) is initialized by sweeping a minor-loop of B_{ip} : B_{ip} is decreased from positive saturation to small negative values until the first switching event occurs (orange/light grey line). Subsequently B_{ip} is returned to 0 (blue/dark grey line) leaving the spin valve in the remanent antiparallel state (R_{AP}). The parallel configuration (b) is prepared similarly by sweeping B_{ip} from saturation field to 0. As no reversal of the electrodes' magnetization occurs at positive B_{ip} for this sweep direction the devices resistance remains in the remanent R_P -state.

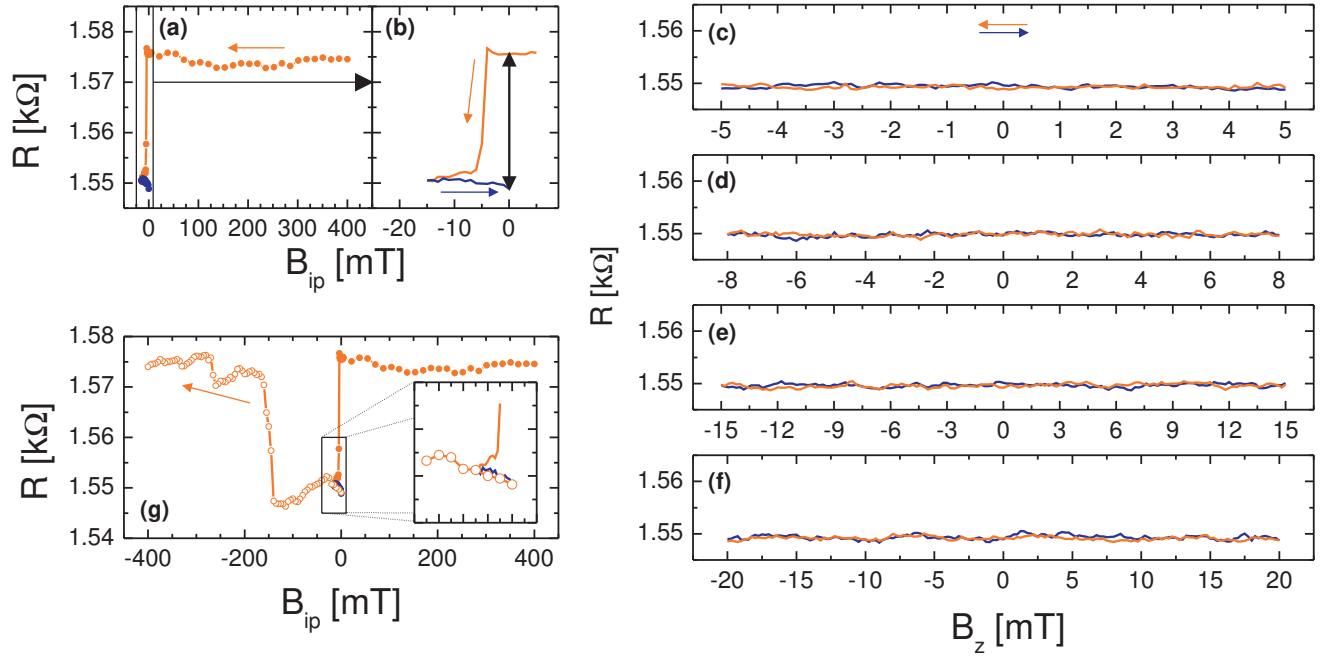


FIG. 4: Sequence of measurements investigating the remanent antiparallel state of a AlQ_3 OSV in a perpendicular magnetic field, recorded at 4.2 K and $U_{bias} = -100\text{ mV}$. The initial minor-loop shown in (a) and (b) necessary for the preparation of the anti-parallel state, exhibits a MR ratio of $\approx -1.7\%$ at $B_{ip} = 0\text{ mT}$. (c)-(f) contain the data of the experiments in the perpendicular geometry. Please note that the scale for R is the same in all plots. The maximum absolute B_z and the corresponding minimum precession time t_{prec} , calculated using Equ. 3, is increased/decreased in every single measurement. We observe a constant device resistance in all measurements (c)-(f) of the series in which the minimum t_{prec} was varied from $\approx 7.1\text{ ns}$ to $\approx 1.8\text{ ns}$. The statistical variations of R in the range of $\approx \pm 0.25\%$ are much smaller than the total magnetoresistance effect. Having finished the measurements in the perpendicular geometry the initial minor-loop measurement is completed with a sweep of B_{ip} from $= 0\text{ mT}$ to large negative values [line with open circles in (g)]. As this scan clearly reproduces the MR scan in Fig. 2(a) we can be sure that the magnetization configuration of the electrodes and by this the spin valve state was not disturbed by applying B_z .

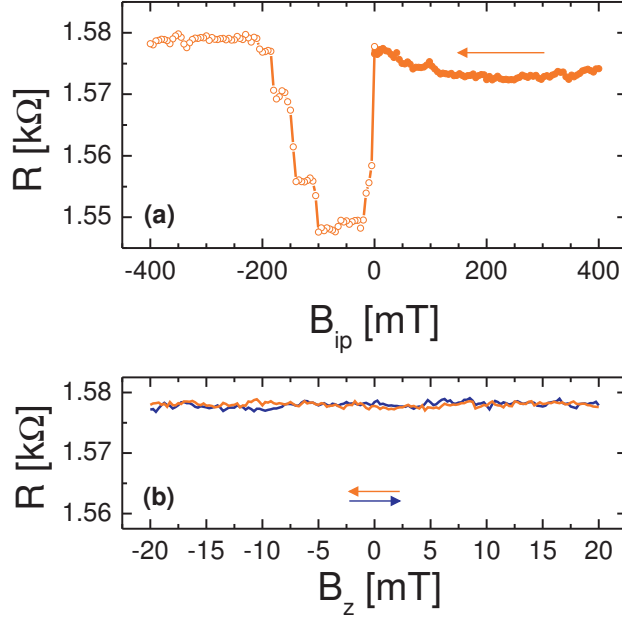


FIG. 5: Results of measurements in the perpendicular geometry for the remanent parallel state of a AlQ_3 OSV recorded at 4.2 K and $U_{bias} = -100\text{ mV}$. A sweep of B_{ip} from high positive fields to $B_{ip} = 0\text{ mT}$ is first performed in order to set the device's state of parallel electrodes' magnetization at $B_{ip} = 0\text{ mT}$ [closed circles in (a)]. (b) shows data of a measurement in a perpendicular magnetic field for maximum $B_z = 20\text{ mT}$ corresponding to a minimum $t_{prec} \approx 1.8\text{ ns}$. As for antiparallel configuration the devices resistance is constant apart from statistical variations in the range of $\approx \pm 0.25\%$. Again the experiment is completed by the termination of the initial MR sweep [open circles in (a)] reproducing the MR trace of the device [Fig. 2(a)].

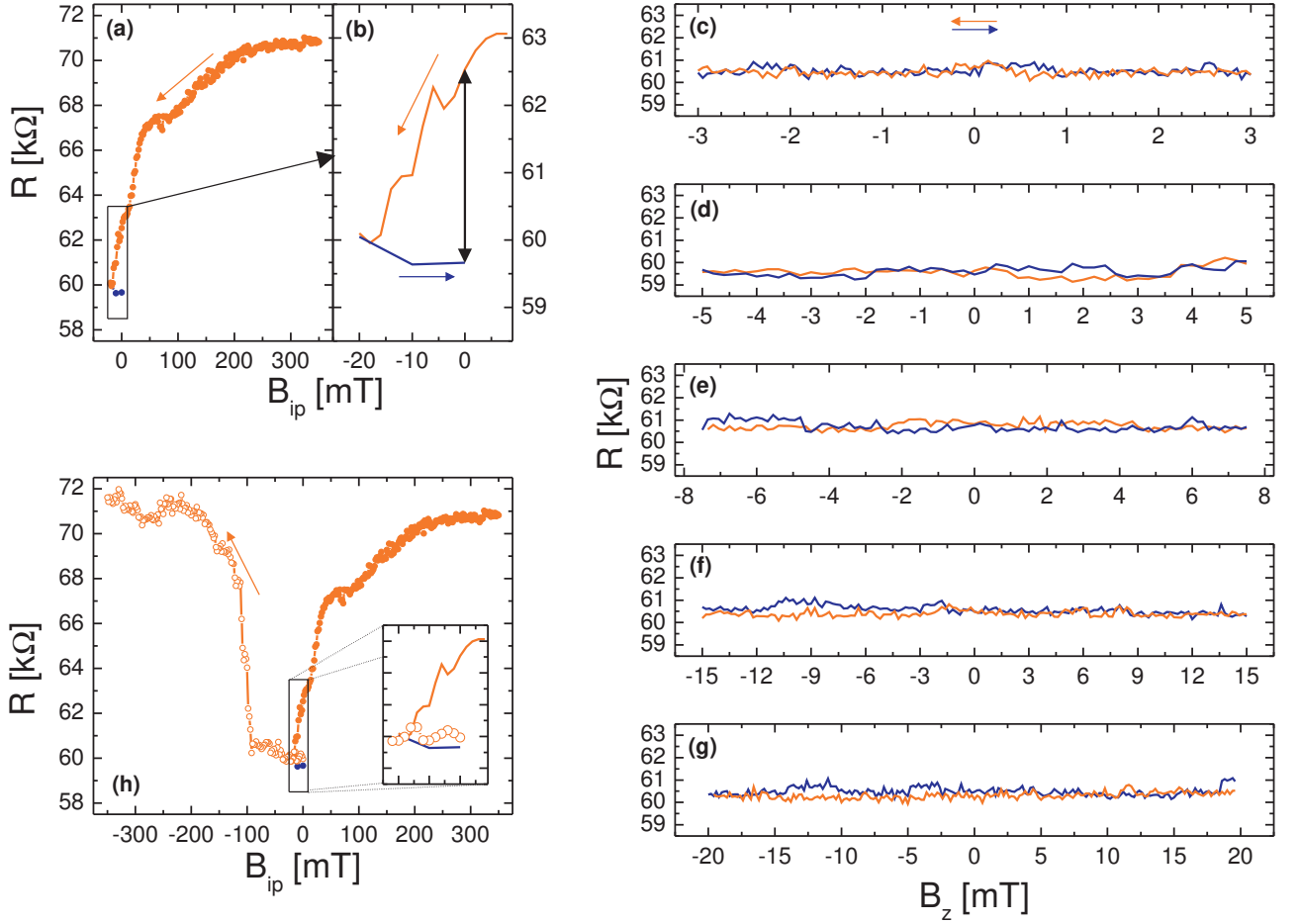


FIG. 6: Complete measurement sequence of an experiment in the perpendicular geometry for the remanent antiparallel state of a PTCDI-C4F7 device recorded at 4.2 K and $U_{bias} = -10\text{ mV}$. (a) and (b) show the minor-loop sweep for the preparation of the antiparallel state with a minor-loop MR ratio of -4.7% at $B_{ip} = 0\text{ mT}$. Fig. (c)-(g) comprise the results of the measurements in perpendicular magnetic fields; again the scale for R in (c)-(g) is the same as in (a) and (h). Measurements at $B_{ip} = 0\text{ mT}$ with different maximum B_z corresponding to minimum spin precession times from $t_{prec} \approx 11.9\text{ ns}$ to $\approx 1.8\text{ ns}$ were performed. t_{prec} is calculated using Equ. 3. As can be seen in (c)-(g) we only observe statistical variations of the resistance in the range of $\approx \pm 1\%$. The sequence is finished by completing the initial minor-loop measurement with a sweep of B_{ip} from $= 0\text{ mT}$ to high negative values [line with open circles in (h)]. This measurement shows that the magnetization state of the electrodes was not disturbed by applying B_z as can be seen from a comparison of the data in (h) with the MR scan in Fig. 2(b).

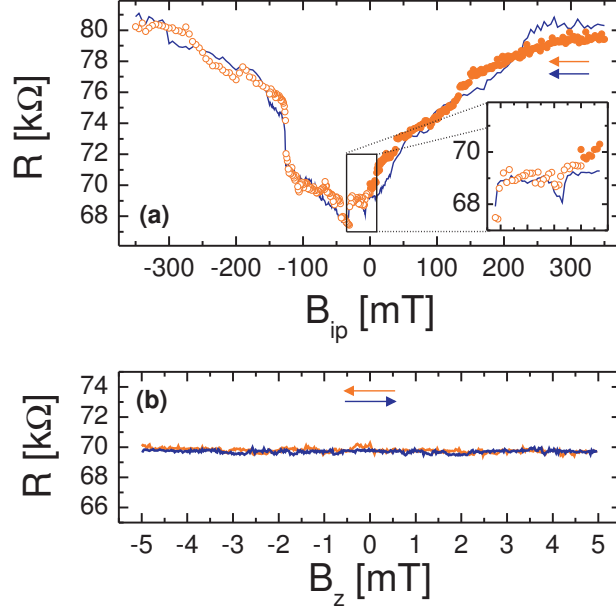


FIG. 7: Experiments with the magnetic field applied perpendicular to the sample plane for the parallel state of a PTCDI-C4F7 device, recorded at 4.2 K and $U_{bias} = -10$ mV. The blue (dark grey) line in the background of panel (a) represents the preliminarily recorded full MR sweep. The state of parallel magnetization of the electrodes is prepared by sweeping B_{ip} from high positive fields to $B_{ip} = 0$ mT [full circles in (a)]. Subsequently the measurements in perpendicular geometry are performed (b). The resistance obtained in a measurement with maximum $B_z = 5$ mT corresponding to a minimum $t_{prec} \approx 7.1$ ns is constant and only variations ($\approx \pm 1\%$) much smaller than the actual spin valve effect are observed. The experiment is finished by the completion of the initial MR sweep [open circles in (a)] verifying that the magnetization state of the electrodes was not modified by the applied B_z . The measured MR trace clearly reproduces the preliminarily recorded curve [blue/dark grey line in (a)].